

Statistical weighting of model-based optoacoustic reconstruction for minimizing artefacts caused by strong acoustic mismatch

X. Luís Deán-Ben, Daniel Razansky* and Vasilis Ntziachristos

Institute for Biological and Medical Imaging, Technical University of Munich and Helmholtz Center Munich, Ingolstädter Landstraße 1, 85764 Neuherberg, Germany.

ABSTRACT

A modified quantitative inversion algorithm is presented that minimizes the effects of internal acoustic reflections or scattering in tomographic optoacoustic images. The inversion procedure in our model-based algorithm consists in solving a linear system of equations in which each individual equation corresponds to a given position of the acoustic transducer and to a given time instant. Thus, the modification that we propose in this work consists in weighting each equation of the linear system with the probability that the measured wave is not distorted by reflection or scattering phenomena. We show that the probability that a reflected or scattered wave is detected at a given position and at a given instant is approximately proportional to the size of the area in which the original wave could have been generated, which is dependent on the position of the transducer and on the time instant, so that such probability can be used to weight each equation of the linear system. Thereby, the contribution of the waves that propagate directly to the transducer to the reconstructed images is emphasized. We experimentally test the proposed inversion algorithm with tissue-mimicking agar phantoms in which air-gaps are included to cause reflections of the acoustic waves. The tomographic reconstructions obtained with the modification proposed herein show a clear reduction of the artefacts due to these acoustic phenomena with respect to the reconstructions yielded with the original algorithm. This performance is directly related to *in-vivo* small animal imaging applications involving imaging in the presence of bones, lungs, and other highly mismatched organs.

Keywords: Optoacoustic tomography, model-based inversion, acoustic mismatch

1. INTRODUCTION

Optoacoustic tomography is an emerging modality that makes use of the optoacoustic effect to image biological samples, with applications in medical and small animal imaging.¹⁻³ The optoacoustic effect consists in the generation of ultrasonic waves due to the thermoelastic expansion caused by light absorption, being short-pulsed lasers employed in common implementations of the technique. The advantages of optoacoustics stem from the combination of optical and ultrasound into a single modality; which allows anatomical, molecular and functional imaging with high optical contrast and a resolution higher than in pure optical techniques for penetration depths higher than the transport mean free path.⁴

The optoacoustic reconstruction consists in the computation of the space-dependent initial pressure (which is proportional to the optical absorbed energy) from the time-resolved pressure signals measured at several positions outside the imaged sample. Several algorithms have been reported in which for simplicity a homogeneous medium with constant speed of sound is assumed,⁵⁻⁸ so that distorted images may be obtained in the presence of acoustic mismatch.

Speed of sound variations of up to 10% can appear inside biological tissues.⁹ Then, it is convenient to modify the acoustic reconstruction algorithms to correct for the associated time-shifting in the pressure signals.¹⁰⁻¹² On the other hand, different phenomena such as reflections or scattering of the acoustic waves take place in regions with a higher acoustic mismatch,^{13,14} in a way that artefacts may appear in the reconstructed images obtained in the presence of lungs, bones or other highly mismatch organs. In a previous work, we introduced a modification

*E-mail: dr@tum.de

of the filtered back-projection algorithm to reduce the artefacts produced in the tomographic reconstructed images when acoustic reflections or scattering take place.¹³ It is based on weighting the contribution of the signal measured at a given transducer position and at a given instant with the probability that a reflected or scattered wave is not measured. Thereby, the reconstruction is made preferably with the "parts" of the signals than more likely correspond to direct wave propagation from the excitation point.

In this work, we demonstrate the applicability of the same statistical approach to the modification of a semi-analytical model-based inversion algorithm, termed interpolated-matrix-model inversion (IMMI).¹⁵ Such algorithm shows a better performance than the filtered back-projection algorithm, specifically avoiding the artefacts in the form of negative values produced with the latter method. Then, it is important to analyse the improvements of the reconstructed images obtained with a modification of IMMI when strong acoustic heterogeneities are present.

The organization of this work is as follows. First, the IMMI algorithm as well as the statistical approach principles are reviewed. Then, the suggested modification of the algorithm is introduced. In the experimental section, we show results obtained with tissue-mimicking phantoms in which air-gaps are included to cause acoustic reflections of the acoustic waves. Finally, some concluding remarks are provided in the final section.

2. THEORY

2.1 Interpolated-matrix-model inversion

The principles of the IMMI algorithm are reviewed in this section. A more detailed description can be found in Ref. 15.

For short-pulsed laser illumination, the pulse duration is usually lower than the thermal confinement time, so that the temporal dependence of the absorbed energy can be approximated by a Dirac delta $\delta(t)$. Under these conditions, the generated pressure field in a homogeneous acoustic medium can be expressed as

$$\frac{\partial^2 p(\mathbf{r}, t)}{\partial t^2} - c^2 \nabla^2 p(\mathbf{r}, t) = \Gamma H(\mathbf{r}) \frac{\partial \delta(t)}{\partial t}, \quad (1)$$

where c is the speed of sound, $H(\mathbf{r})$ is the amount of energy absorbed in the tissue per unit volume and Γ is the Grueneisen parameter (dimensionless). A solution of Eq. 1 is given by the Poisson-type integral as

$$p(\mathbf{r}, t) = \frac{\Gamma}{4\pi c} \frac{\partial}{\partial t} \int_{S'} \frac{H(\mathbf{r}')}{|\mathbf{r} - \mathbf{r}'|} dS', \quad (2)$$

where S' is the surface of a sphere centred at \mathbf{r} and with a radius equal to ct . In a two-dimensional geometry, for which all the sources lie in a plane, the integration in Eq. 2 is performed over a circumference. Thereby, for a given sensor position $\mathbf{r} = (x_0, y_0)$, the integral in Eq. 2 can be explicitly rewritten as

$$\int_{S'} \frac{H(\mathbf{r}')}{|\mathbf{r} - \mathbf{r}'|} dS' = \int_{\theta_1}^{\theta_2} H(x_0 + R \cos \theta, y_0 + R \sin \theta) d\theta, \quad (3)$$

where θ denotes the angle on the circle, and θ_1 and θ_2 denote the angles of the two intersections of the circle with the square region in which $H(\mathbf{r}')$ is reconstructed (Fig. 1). In practice, a discrete image is reconstructed in which the spatial sampling of $H(\mathbf{r}')$ is equal to the pixel size, so a discrete approximation of Eq. 2 can be used, i.e.:

$$p(\mathbf{r}_i, t_j) = \sum_{k=1}^N a_k^{ij} H(\mathbf{r}'_k) \quad (4)$$

being N the number of pixels of the image. To calculate the coefficients a_k^{ij} from Eqs. 2 and 3, interpolated values of $H(\mathbf{r}')$ must be calculated along the circumference in which Eq. 3 is computed. It has been shown in Ref. 15 the convenience of performing the interpolation by tiling the x-y reconstruction plane with right-angle triangles with vertexes on the grid point as illustrated in Fig. 1. Then, the value of $H(\mathbf{r}')$ is obtained by linear interpolation inside each triangle.

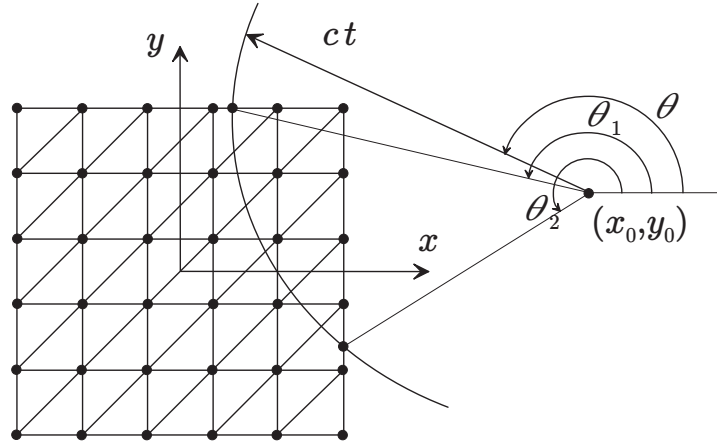


Figure 1. Grid of points corresponding to the position of the pixels of the reconstructed image. The reconstruction plane is tiled with right-angle triangles so that the absorbed energy is obtained by linear interpolation inside each triangle. The curve along which the integral in Eq. 3 is calculated is shown for a certain transducer located at (x_0, y_0) and for a given instant t .

The same discretization of Eq. 2 can be obtained for M positions of the transducer and for L instants, in a way that a system of linear equations can be formulated, which is expressed in a matrix form as

$$\mathbf{p} = \mathbf{A}\mathbf{H} \quad (5)$$

Eq. 5 corresponds to the forward model, in which the theoretical pressure for a set of detector positions and instants \mathbf{p} is calculated as a function of the absorbed energy in the pixel positions \mathbf{H} . The optoacoustic reconstruction is performed by minimizing the mean square difference between the theoretical pressure \mathbf{p} and the measured pressure \mathbf{p}_m , i.e.:

$$\mathbf{H}_{\text{sol}} = \underset{\mathbf{H}}{\operatorname{argmin}} \|\mathbf{p}_m - \mathbf{A}\mathbf{H}\|^2 \quad (6)$$

The solution of Eq. 6 is calculated by means of the LSQR algorithm, in which the sparsity of the model matrix is exploited to make a fast reconstruction.

2.2 Probability of distortion of the signals due to reflection or scattering events

In this section we review the estimation of the probability that the signal measured at a given detector position and at a given instant is not affected by acoustic reflection or scattering events. A more detailed description can be found in Ref. 14, where we used this approach to modify the filtered back-projection algorithm in order to minimize these effects in the tomographic reconstructions.

In optoacoustic reconstruction algorithms, usually a homogenous medium with constant speed of sound is assumed, which is equivalent to considering direct wave propagation between the excitation and measuring points. However, if strong heterogeneities are present, there is a possibility that the signal measured at a given detector position and at a given point is distorted by a reflected or scattered acoustic wave.

To estimate the probability that a reflected or scattered wave is measured at a given detector position and at a given instant, we assume a 2D domain in which we can determine an area A (grey area in Fig. 2) containing all the optical absorbers (points in which $H(\mathbf{r}') \neq 0$) and all the possible acoustic reflectors and acoustic scatterers. The probability $P_r^i(t_j)$ of detecting a reflected or scattered wave with unit amplitude (in arbitrary units) at the i -th position of the transducer \mathbf{r}_i and at time t_j is given by

$$P_r^i(t_j) = \int_{A_{ij}} P_r^i(t_j|\mathbf{r}') f_E(\mathbf{r}') d\mathbf{r}' \quad (7)$$

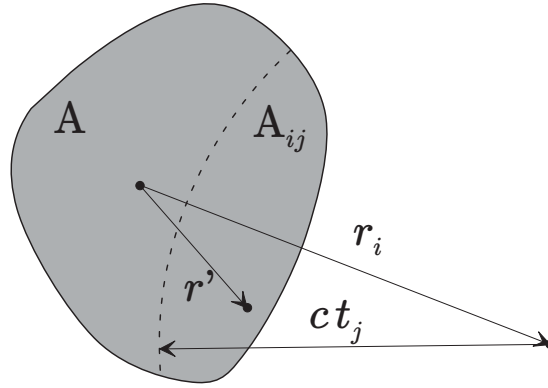


Figure 2. Principle underlying the statistical weighting approach. The area A is an area containing all the optical absorbers and all the possible acoustic reflectors and acoustic scatterers. The area A_{ij} contains all the points \mathbf{r}' in which a reflected or scattered wave may have been generated to be detected at the transducer located in \mathbf{r}_i at instant t_j .

begin $f_E(\mathbf{r}')$ the probability density function corresponding to the location at which a differential of energy is absorbed and $P_r^i(t_j|\mathbf{r}')$ the conditional probability that a reflected or scattered wave with unit amplitude is detected at instant t_j given that all the energy is absorbed at \mathbf{r}' . If a *priori* information about the position of the absorbers does not exist, $f_E(\mathbf{r}')$ corresponds to a uniform distribution, so that

$$P_r^i(t_j) = \frac{A_{ij}}{A} \int_{A_{ij}} P_r^i(t_j|\mathbf{r}') d\mathbf{r}', \quad (8)$$

where A_{ij} is the area inside A covered by a circle of radius ct_j centred at the transducer position (Fig. 2). We define $P_{r,dist}^i(t_j)$ as the probability that the wave measured with the i -th transducer at instant t_j is distorted by a reflected or scattered wave. In practice, such distortion is produced when the scattered or reflected wave is above the noise level, so that $P_{r,dist}^i(t_j)$ is proportional to $P_r^i(t_j)$. We have shown in Ref. 14 that $P_{r,dist}^i(t_j)$ can be expressed as

$$P_{r,dist}^i(t_j) = \min \left(1, \omega \frac{A_{ij}}{A} \right), \quad (9)$$

where ω is a weighting parameter to be determined heuristically. Then, the probability $P_d^i(t_j)$ that the signal detected by the i -th transducer at instant t_j corresponds to a direct propagation, i.e., that it is not distorted by reflection or scattering events, is given by

$$P_d^i(t_j) = 1 - P_{r,dist}^i(t_j). \quad (10)$$

2.3 Weighted interpolated-matrix-model inversion

The modification of the IMMI algorithm suggested in this work consists in weighting the contribution of each transducer position and each instant with the probability that the signal is not distorted by a reflected or scattered wave. Thereby, the reconstruction is preferably made with the "parts" of the signals that more likely correspond to a direct propagation between the excitation and detection points.

Then, taking into account that each equation of the linear system (Eq. 4) corresponds to a given position of the transducer and to a given instant, the equations are weighted with the value of $P_d^i(t_j)$, i.e., Eq. 4 is modified as

$$P_d^i(t_j) p(\mathbf{r}_i, t_j) = P_d^i(t_j) \sum_{k=1}^N a_k^{ij} H(\mathbf{r}'_k), \quad (11)$$

In this way, the linear system of equations in Eq. 5 is modified as

$$\mathbf{W}\mathbf{p} = \mathbf{WA}\mathbf{H}, \quad (12)$$

being \mathbf{W} a diagonal matrix with elements $P_d^i(t_j)$.

The reconstruction is then made by solving a mean square difference minimization problem equivalent to Eq. 6, which is given by

$$\mathbf{H}_{\text{sol}} = \underset{\mathbf{H}}{\operatorname{argmin}} \|\mathbf{W}\mathbf{p}_m - \mathbf{WA}\mathbf{H}\|^2. \quad (13)$$

3. EXPERIMENT

3.1 Experimental setup

The experimental system used to test the proposed method consisted of an optical parametric oscillator (OPO)-based laser (MOPO series, Spectra Physics), pumped by a nanosecond pulsed Nd:YAG laser (Lab-190-30, Spectra Physics) with 15 Hz pulse repetition, which is used as the illuminating source. The wavelength in the experiments was set to 605 nm. The output beam was split into two parts and directed through a linear light diffuser onto the object from two opposite sides to attain a ring-type uniform illumination conditions on the surface of the object. The generated ultrasonic waves were detected with a high-sensitivity cylindrically-focused ultrasonic immersion PZT transducer (model V382, Panametrics-NDT) with a central frequency of 3.5 MHz and a focal length of 38.1 mm. The acquired time-resolved signals were amplified and digitalized by an embedded oscilloscope card at a sampling rate of 100 MSPS (NI PCI-5122, National Instruments) and 14 bit resolution. The samples were rotated with a high speed rotation stage (Thorlabs PRM1/MZ7), so that the signals were acquired for 180 tomographic projections with angular steps of 2° . For each projection, the signal was averaged 64 times and a band-pass filter with cutoff frequencies 0.1 MHz and 5 MHz was applied. A more detailed description of the experimental system can be found in Ref. 16.

3.2 Phantoms

Several phantoms made with agar (1.3% agar powder by weight) were used in the experiment. First, a pure agar phantom was prepared to illustrate the nature of the artefacts caused by acoustic reflections. In this phantom, we included a cylindrical hollow cavity and an absorbing region with 0.012% by volume of black India ink, which corresponds to an optical absorption coefficient of $\mu_a = 1.2 \text{ cm}^{-1}$. Other phantoms were prepared in which we simulated the background absorption and background scattering of tissue. For this, we added, respectively, 0.002% by volume of black India ink and 1.2% by volume of Intralipid to the agar solution. This corresponds approximately to an absorption coefficient $\mu_a = 0.2 \text{ cm}^{-1}$ and a reduced scattering coefficient $\mu'_s = 10 \text{ cm}^{-1}$.¹⁷ Hollow cylindrical cavities were included in the phantoms in order to cause acoustic reflections of the waves. Also, regions with higher optical absorption were added, in which the concentration of black ink is 0.01% by volume, corresponding to an optical absorption coefficient $\mu_a = 1 \text{ cm}^{-1}$.

3.3 Experimental results

The results of the first experiment corresponding to the agar phantom with no background absorption and no background scattering are displayed in Fig. 3. Fig. 3a shows the tomographic reconstruction obtained with the original IMMI algorithm, which exemplifies the typical artefacts produced in the images due to acoustic reflections or scattering. Indeed, the dark halo surrounding the cylindrical cavity is originated due to the assumption that the reflected waves propagate directly to the transducer from the excitation point. Also in Fig. 3a, a circumference covering the object is indicated with a white dashed line, which limits the area A used in the modified algorithm. Then, in Figs. 3b, 3c, 3d and 3e the results obtained with the modified IMMI algorithm are displayed for weighting factors $\omega = 0.33$, $\omega = 0.66$, $\omega = 1$ and $\omega = 1.5$ respectively. It is shown that the artefacts are reduced when increasing the weighting parameter, and almost disappear for $\omega = 1$. No significant improvement is obtained when using weighting parameters higher than 1. For example, there is no significant reduction of artefacts in Fig. 3e with respect to Fig. 3d, whereas the region around the optical absorber appears more distorted. This indicates that, as well as in the method proposed in Ref. 14, it appears to be convenient to use a weighting factor equal to 1 in the reconstruction.

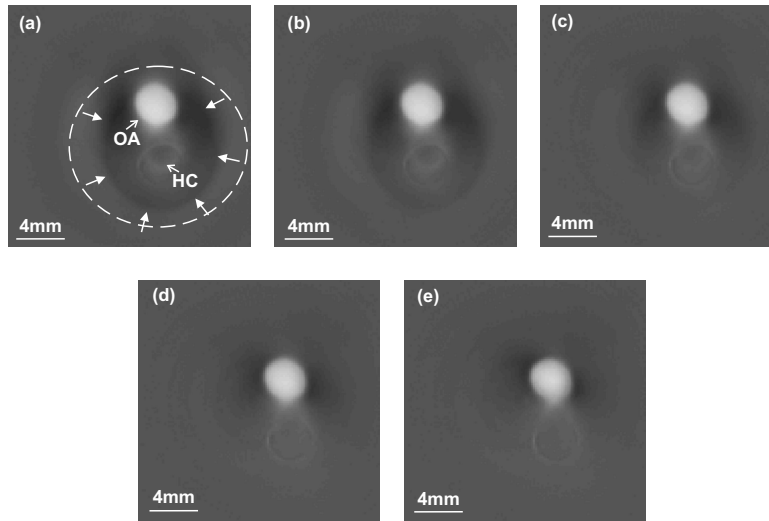


Figure 3. Tomographic reconstructions of an agar phantom with an optical absorber (OA) and a hollow cavity (HC). The tomographic reconstruction obtained with the IMMI algorithm is shown in (a). The artefacts due to the reflection of the acoustic waves at the hollow cavity are indicated with white arrows. The tomographic reconstructions obtained with the weighted IMMI algorithm proposed in this work for $\omega = 0.33$, $\omega = 0.66$, $\omega = 1$ and $\omega = 1.5$ are shown in (b), (c), (d) and (e) respectively. The area A is taken as the area limited by the dashed circumference in (a).

The results obtained in the experiments with tissue-mimicking phantoms are displayed in Fig. 4. Specifically, we show a comparison between the tomographic reconstructions obtained, respectively, with the original IMMI algorithm and with the weighted IMMI algorithm presented in this work. The weighting parameter considered in the modified algorithm corresponds to $\omega = 1$ and the area A is taken as the circle inscribed in the region of interest. The artefacts due to the reflections of the acoustic waves are indicated with arrows in the images. It is shown that a reduction of such artefacts is achieved with the modified IMMI algorithm for all the cases.

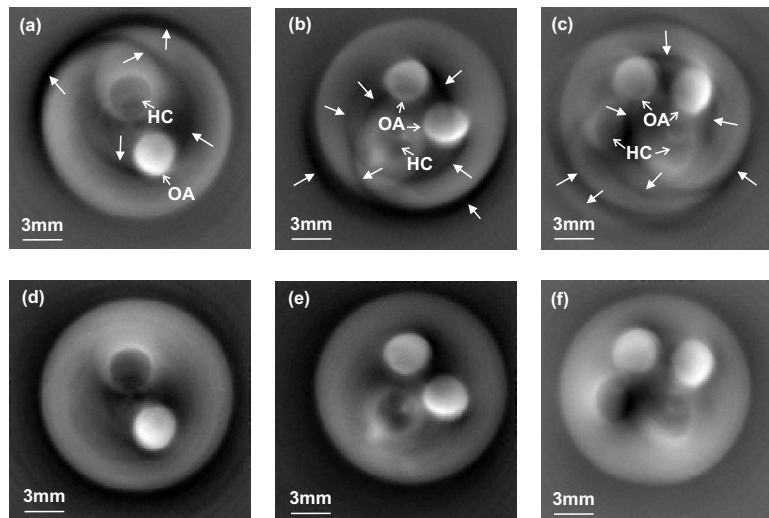


Figure 4. Tomographic reconstructions of tissue-mimicking phantoms in which optical absorbers (OA) and hollow cavities (HC) are included. The tomographic reconstructions obtained with the IMMI algorithm are shown in (a), (b) and (c) and the tomographic reconstructions obtained with the weighted IMMI algorithm proposed in this work are shown, respectively, in (d), (e) and (f). The artefacts due to the reflection of the acoustic waves in the hollow cavities are indicated with white arrows in (a), (b) and (c). The area A is taken as the circle inscribed in the region of interest.

4. CONCLUSIONS

We have introduced a modification of a quantitative inversion algorithm that minimizes the effects of internal acoustic reflections or scattering in tomographic photoacoustic images. In the original algorithm, the reconstruction is done by solving a linear system of equations. Then, we proposed a modification of this algorithm in which each equation of the linear system, which correspond to a given transducer position and to a given instant, is weighted with the probability that the corresponding signal is not distorted by a reflected or scattered acoustic wave. Performance tests were shown in agar phantoms in which hollow cylindrical cavities were included to cause reflections of the acoustic waves. The tomographic reconstructions obtained with the modification proposed herein show a clear reduction of the artefacts due to these acoustic phenomena with respect to the reconstructions yielded with the original algorithm, which indicates its convenience to compute the reconstructions in regions with highly mismatched organs.

ACKNOWLEDGMENTS

Daniel Razansky acknowledges support from the German Research Foundation (DFG) Research Grant (RA 1848/1). Vasilis Ntziachristos acknowledges support from the ERC Senior Investigator Award and the Medizin Technik BMBF award for excellence in medical innovation.

REFERENCES

- [1] Wang, X., Pang, Y., Ku, G., Xie, X., Stoica, G., and Wang, L. V., "Noninvasive laser-induced photoacoustic tomography for structural and functional *in vivo* imaging of the brain," *Nature Biotechnology* **21**(7), 803–806 (2003).
- [2] Razansky, D., Distel, M., Vinegoni, C., Ma, R., Perrimon, N., Köster, R. W., and Ntziachristos, V., "Multispectral opto-acoustic tomography of deep-seated fluorescent proteins *in vivo*," *Nature Photonics* **3**(7), 412–417 (2009).
- [3] Wang, L. V., ed., [*Photoacoustic Imaging and Spectroscopy*], CRC Press, Boca Raton (USA) (2009).
- [4] Ntziachristos, V., "Going deeper than microscopy: the optical imaging frontier in biology," *Nature Methods* **7**(8), 603–614 (2010).
- [5] Kruger, R. A., Liu, P., Fang, Y., and Appledorn, C. R., "Photoacoustic ultrasound PAUS - reconstruction tomography," *Medical Physics* **22**(10), 1605–1609 (1995).
- [6] Köstli, K. P., Frauchiger, D., Niederhauser, J. J., Paltauf, G., Weber, H. P., and Frenz, M., "Optoacoustic imaging using a three-dimensional reconstruction algorithm," *IEEE Journal of Selected Topics in Quantum Electronics* **7**(6), 918–923 (2001).
- [7] Norton, S. J. and Vo-Dinh, T., "Optoacoustic diffraction tomography: analysis of algorithms," *Journal of the Optical Society of America A* **20**(10), 1859–1866 (2003).
- [8] Xu, M. and Wang, L. V., "Universal back-projection algorithm for photoacoustic computed tomography," *Physical Review E* **71**(1), 016706 (2005).
- [9] Szabo, T. L., [*Diagnostic Ultrasound Imaging: Inside Out*], Elsevier Academic Press, San Diego (USA) (2004).
- [10] Xu, Y. and Wang, L. V., "Effects of acoustic heterogeneity in breast thermoacoustic tomography," *IEEE Transactions on Ultrasonics, Ferroelectrics and Frequency Control* **50**(9), 1134–1146 (2003).
- [11] Jin, X. and Wang, L. V., "Thermoacoustic tomography with correction for acoustic speed variations," *Physics in Medicine and Biology* **51**(24), 6437–6448 (2006).
- [12] Jiang, H., Yuan, Z., and Gu, X., "Spatially varying optical and acoustic property reconstruction using finite-element-based photoacoustic tomography," *Journal of the Optical Society of America A* **23**(4), 878–888 (2006).
- [13] Cox, B. T. and Treeby, B. E., "Artifact trapping during time reversal photoacoustic imaging for acoustically heterogeneous media," *IEEE Transactions on Medical Imaging* **29**(2), 387–396 (2010).
- [14] Deán-Ben, X. L., Ma, R., Razansky, D., and Ntziachristos, V., "Statistical approach for optoacoustic image reconstruction in the presence of strong acoustic heterogeneities," *IEEE Transactions on Medical Imaging* . DOI:10.1109/TMI.2010.2081683.

- [15] Rosenthal, A., Razansky, D., and Ntziachristos, V., “Fast semi-analytical model-based acoustic inversion for quantitative optoacoustic tomography,” *IEEE Transactions on Medical Imaging* **29**(6), 1275–1285 (2010).
- [16] Ma, R., Taruttis, A., Ntziachristos, V., and Razansky, D., “Multispectral optoacoustic tomography (MSOT) scanner for whole-body small animal imaging,” *Optics Express* **17**(24), 21414–21426 (2009).
- [17] Razansky, D. and Ntziachristos, V., “Hybrid photoacoustic fluorescence molecular tomography using finite-element-based inversion,” *Medical Physics* **34**(11), 4293–4301 (2007).